Travelling Waves of the Diffusive Streeter-Phelps Equations with Braun-Berthouex BOD Decay

Alexandra Lawryshyn*

Project Advisor: Dr. Hermann J. Eberl†

Abstract. In this paper, we study the diffusive Streeter-Phelps equations, consisting of two weakly coupled diffusion-advection-reaction equations that describe biological oxygen demand (BOD) and dissolved oxygen (DO) in a river. The Streeter-Phelps equations were first introduced in 1925 but are still used in river quality modelling to this day. We investigate travelling wave solutions to this system with non-linear BOD decay instead of traditional linear decay. We prove the existence of spectrally stable monotone wavefront solutions to the BOD equation and corresponding solutions to the DO equation. We also discuss the existence and instability of non-monotone travelling waves and give an approximation of stable solutions to the BOD equation. Our analytical findings are illustrated numerically.

1. Introduction.

Biological oxygen demand (BOD) and dissolved oxygen (DO) are important indicators of river water quality, and are often studied through the use of mathematical models. BOD is defined as the amount of oxygen required for microorganisms to break down an organic pollutant in a body of water. BOD concentration is therefore proportional to the amount of pollution in a river. When a pollutant enters a river, microorganisms such as bacteria break down the pollutant through aerobic metabolic processes, using up oxygen. Thus, there is a spike in BOD at the instant the pollutant enters the river. As the bacteria break down the pollutant, oxygen is consumed, leading to a rapid decrease of DO and a gradual decay of BOD. After a certain period of time (usually on the order of days), the pollutant is fully degraded and DO and BOD concentrations gradually return to their natural levels. This process is illustrated by the Streeter-Phelps [15] oxygen sag curve shown in Figure 1.1.

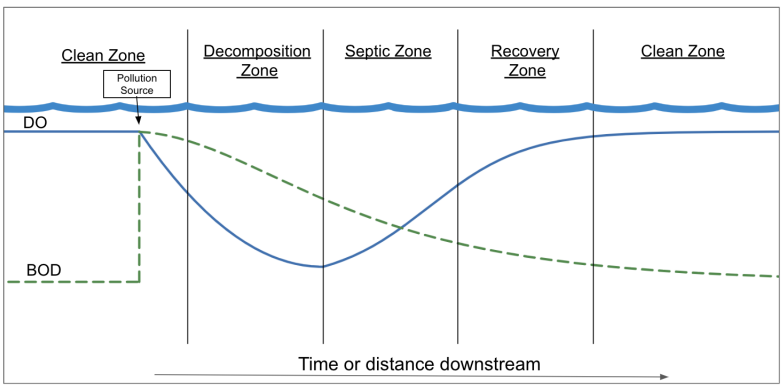

Figure 1.1. *A visual depiction of the Streeter-Phelps oxygen-sag curve, showing how BOD and DO levels in a river are affected by the addition of a pollutant.*

*Department of Mathematics and Statistics, University of Guelph, (alawrysh@uoguelph.ca).
†Department of Mathematics and Statistics, University of Guelph

A model of two diffusion-advection-reaction equations introduced in [4] is commonly used to describe the interaction between BOD and DO concentrations in a flowing river. The model is given by

$$\frac{\partial b}{\partial t} + v\frac{\partial b}{\partial x} = K\frac{\partial^2 b}{\partial x^2} - k_3 b + b_a, \tag{1.1}$$

$$\frac{\partial c}{\partial t} + v\frac{\partial c}{\partial x} = K\frac{\partial^2 c}{\partial x^2} - k_1 b + k_2(c_s - c), \tag{1.2}$$

where b and c are BOD and DO concentrations respectively, v is the average river velocity, K is the diffusion constant, k_1, k_2 and k_3 describe DO decay, BOD decay, and re-aeration rates respectively, b_a is the BOD addition rate, and c_s is the DO saturation level. Also, $x \in \mathbb{R}$ and $t > 0$ represent the space and time coordinates, respectively. While molecular diffusion is often negligible in river quality modelling, diffusion terms are included to describe longitudinal and turbulent dispersion [10]. Longitudinal dispersion describes the spreading of particles in the same direction as the river, whereas turbulent dispersion refers to particles spreading within the cross-sectional area of the river.

Equations (1.1) and (1.2) are one-way coupled through a linear reaction rate proposed in [15] that describes BOD decay due to an organic pollutant entering the river. This model, however, does not fit BOD data that exhibit an initial lag phase on the deoxygenation curve. This initial delay in BOD degradation is commonly observed experimentally, likely as a result of bacterial growth kinetics [2]. To account for this process, [2] proposed an alternate BOD decay term following Monod kinetics [12]. The decay term is given in dimensionless form by

$$g(b) := \frac{b(1-b)}{\kappa + b} \tag{1.3}$$

where b is dimensionless BOD concentration and κ is a positive dimensionless constant representing the half-saturation concentration level. With this reaction term in place of the traditional linear decay term, (1.1) and (1.2) become

$$\frac{\partial b}{\partial t} + P\frac{\partial b}{\partial x} = \frac{\partial^2 b}{\partial x^2} - Dg(b), \tag{1.4}$$

$$\frac{\partial c}{\partial t} + P\frac{\partial c}{\partial x} = \frac{\partial^2 c}{\partial x^2} - \hat{D}g(b) + S(1-c), \tag{1.5}$$

in dimensionless form. Here, c is the dimensionless DO concentration and

$$P = \frac{\text{advection rate}}{\text{diffusion rate}}, \quad D = \frac{\text{reaction rate}}{\text{diffusion rate}}, \quad S = \frac{\text{total mass transfer rate}}{\text{diffusion rate}}$$

are the positive dimensionless Péclet, Damköhler II, and Sherwood numbers, respectively. Also, $\hat{D} = \frac{b_s}{c_s}D$ where b_s is the BOD concentration saturation level. The non-dimensionalization leading to (1.4) and (1.5) is given in Appendix A.

The non-linearity of (1.3) gives rise to multiple steady states in the model, suggesting the potential existence of travelling wave solutions which do not arise from the traditional linear model. The objective of this paper is to determine the wave speeds for which (1.4) and (1.5) permit stable travelling wave solutions.

This paper is organized as follows. In section 2, we derive the travelling wave equations for (1.4) and (1.5). Then, we prove the existence of travelling wave solutions to (1.4) and (1.5) in section 3 and section 4, respectively. The spectral stability of these solutions is shown in section 5, and in section 6, we give an analytical approximation of solutions to (1.4). Finally, a discussion of our results and the connection between (1.4) and the generalized Fisher-KPP (F-KPP) equation [6], [9] is given in section 7. Numerical results are given throughout the paper, where we used MATLAB's ode45 and pdepe solvers [16] to produce numerical solutions to the ordinary differential equations (ODEs) and partial differential equations (PDEs), respectively.

2. Derivation of Travelling Wave Equations. Travelling waves are solutions to PDEs that maintain their shape while propagating through space and time with constant speed. They arise from reaction terms that permit steady states of the model. Travelling wave solutions depend solely on the combination of x and t defined by $z := x - \rho t$ where ρ is a constant wave speed. It is assumed without loss of generality that $\rho > 0$, and thus, due to the definition of z, waves travel downstream in the positive direction along the z-axis. Travelling waves commonly arise in the form of wavefronts or pulses, as illustrated in Figure 2.1.

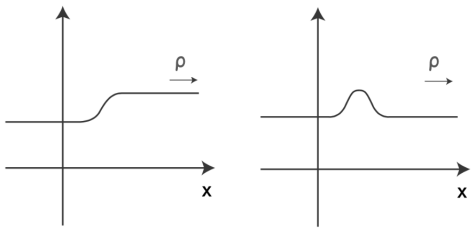

Figure 2.1. *A wavefront (left) and a pulse (right)*

The study of travelling waves solutions to (1.4) and (1.5) begins with imposing the ansatz,

$$z := x - \rho t, \qquad b(x,t) = B(z), \qquad \text{and} \qquad c(x,t) = C(z)$$

which converts the PDE system to the ODE system,

$$B''(z) + \hat{\rho} B'(z) = Dg(B(z)), \tag{2.1}$$

$$C''(z) + \hat{\rho} C'(z) = \hat{D} g(B(z)) - S(1 - C(z)). \tag{2.2}$$

Here, $\hat{\rho} := \rho - P$ represents the difference between the speed of wave propagation and the speed of the river and $g(B)$ was defined by (1.3). The travelling wave equations (2.1) and (2.2) are subject to the following asymptotic boundary conditions:

$$\lim_{z \to \pm\infty} g(B(z)) = 0, \quad \lim_{z \to \pm\infty} B'(z) = 0, \tag{2.3}$$

$$\lim_{z \to \pm\infty} C(z) = 1, \quad \lim_{z \to \pm\infty} C'(z) = 0. \tag{2.4}$$

These conditions ensure that solutions to the travelling wave equations asymptotically connect the rest states of the model.

3. Existence of Travelling Waves.

The existence of travelling wave solutions to (1.4) is guaranteed through its connection to the generalized F-KPP equation, discussed in section 7. Here, we include the complete analysis specific to (1.4).

To show the existence of travelling waves, we look for either heteroclinic or homoclinic trajectories that asymptotically connect equilibria in the phase plane. These trajectories correspond to solutions of (2.1) that satisfy (2.3). By defining $V(z) := B'(z)$, (2.1) can be written as a system of two first order ODEs,

$$B'(z) = V(z), \tag{3.1}$$

$$V'(z) = -\hat{\rho}V(z) + D\frac{B(z)(1-B(z))}{\kappa + B(z)}. \tag{3.2}$$

By setting $B'(z) = 0$ and $V'(z) = 0$, we find equilibria of $(B, V) = (0, 0)$ and $(B, V) = (1, 0)$. The Jacobian matrices are obtained for each equilibrium as

$$\mathbf{J}_{(0,0)} = \begin{pmatrix} 0 & 1 \\ \frac{D}{\kappa} & -\hat{\rho} \end{pmatrix} \quad \text{and} \quad \mathbf{J}_{(1,0)} = \begin{pmatrix} 0 & 1 \\ -\frac{D}{\kappa+1} & -\hat{\rho} \end{pmatrix}$$

with corresponding eigenvalues,

$$\lambda_{(0,0)} = \frac{-\hat{\rho} \pm \sqrt{\hat{\rho}^2 + \frac{4D}{\kappa}}}{2} \quad \text{and} \quad \lambda_{(1,0)} = \frac{-\hat{\rho} \pm \sqrt{\hat{\rho}^2 - \frac{4D}{\kappa+1}}}{2}. \tag{3.3}$$

The Jacobian of the equilibrium at $(0, 0)$ has real eigenvalues of opposite sign for any value of $\hat{\rho}$, so $(0, 0)$ is a saddle point in the phase plane. The classification of $(1, 0)$ however, depends on the relative sizes of $\hat{\rho}$ and $\rho^* := 2\sqrt{\frac{D}{\kappa+1}}$, as summarized in Table 3.1. The following subsections are devoted to studying the existence of travelling waves for each case. For the sake of intuition, we start with the case where $(1, 0)$ is a stable node, followed by the case of an unstable node. We then look at the cases where $(1, 0)$ is a centre or spiral.

Table 3.1
Local stability of $(B, V) = (1, 0)$ for different wave speeds

Value of $\hat{\rho}$	Sign of Eigenvalues	Classification of (1,0)
$\hat{\rho} \leq -\rho^*$	Both positive	Unstable Node
$-\rho^* < \hat{\rho} < 0$	Both complex with $Re(\lambda) > 0$	Unstable Spiral
$\hat{\rho} = 0$	Complex conjugates	Centre
$0 < \hat{\rho} < \rho^*$	Both complex with $Re(\lambda) < 0$	Stable Spiral
$\hat{\rho} \geq \rho^*$	Both negative	Stable Node

3.1. Case 1: $\hat{\rho} \geq \rho^*$.

When $\hat{\rho} \geq \rho^*$, travelling waves, if they exist, travel sufficiently faster than the river ($\rho \geq P + \rho^*$). The phase portrait arising from (3.1) and (3.2) consists of a saddle point at $(0, 0)$ and a stable node at $(1, 0)$, so we search for a trajectory that leaves the unstable manifold of $(0, 0)$ and converges to $(1, 0)$. To prove the existence of this trajectory, we construct a positively invariant triangular region as shown in Figure 3.1. This method was

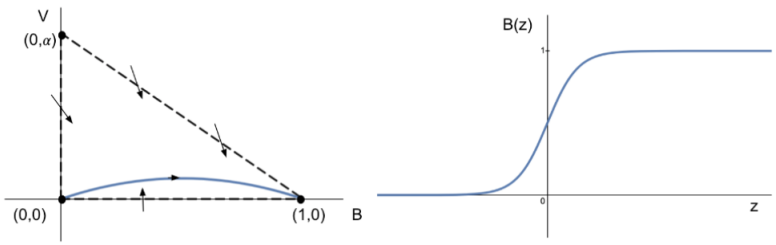

Figure 3.1. *Illustrations of a positively invariant trapping region enclosing a heteroclinic trajectory connecting* $(0,0)$ *to* $(1,0)$ *(left) and the corresponding travelling wave (right).*

outlined, for instance, in [7] for the case of the F-KPP equation. The vertices of the region are $(0,0)$, $(1,0)$, and $(\alpha,0)$ where α is an unknown positive constant. For the region to be positively invariant, the vector field of solutions in the phase plane must point into the region along the entire boundary. Along $V=0$ with $0<B<1$,

$$\begin{aligned} B' &= 0, \\ V' &= D\frac{B(1-B)}{\kappa+B} > 0 \end{aligned}$$

so trajectories point vertically upwards into the region. Along $B=0$ with $V>0$,

$$\begin{aligned} B' &= V > 0, \\ V' &= -\hat{\rho}V < 0 \end{aligned}$$

so trajectories point downwards and to the right, thus entering the region. Along the third line segment defining the boundary, $V=\alpha(1-B)$ with $0<B<1$, we have

$$\begin{aligned} B' &= \alpha(1-B) > 0, \\ V' &= -\hat{\rho}\alpha(1-B) + D\frac{B(1-B)}{\kappa+B} \end{aligned}$$

so trajectories point to the right. For trajectories to enter the region along this line segment, we must choose a value for α so that the vector field points downwards at a slope steeper than the slope of the boundary line. Mathematically, this means we need a value of α such that $\frac{dV}{dB} < -\alpha$. The slope of the vector field along $V=\alpha(1-B)$ is

$$\frac{dV}{dB} = -\hat{\rho} + \frac{DB}{\alpha(\kappa+B)}$$

by the chain rule. So we require

$$\begin{aligned} &-\hat{\rho}+\frac{DB}{\alpha(\kappa+B)}<-\alpha \\ \iff &\alpha^2-\hat{\rho}\alpha+\frac{DB}{\kappa+B}<0 \\ \iff &\alpha\in\left(\frac{\hat{\rho}-\sqrt{\hat{\rho}^2-4\frac{DB}{\kappa+B}}}{2},\frac{\hat{\rho}+\sqrt{\hat{\rho}^2-4\frac{DB}{\kappa+B}}}{2}\right). \end{aligned} \tag{3.4}$$

Choosing $\alpha=\frac{\hat{\rho}}{2}$ for example, results in a boundary line with a slope less steep than the slope of the vector field along the line. Notice that the bounds on α as in (3.4) are imaginary when $\hat{\rho}<2\sqrt{\frac{DB}{\kappa+B}}$, but we will now show that this cannot happen in the region of interest, and is thus not an issue. In this case, we have $\hat{\rho}\geq 2\sqrt{\frac{D}{\kappa+1}}$ and we know $2\sqrt{\frac{DB}{\kappa+B}}=2\sqrt{\frac{D}{\kappa+1}}$ only when $B=1$. If we define $f(B):=2\sqrt{\frac{DB}{\kappa+B}}$, then $f'(B)>0$ so $f(B)$ increases monotonically for all $B>0$. Thus, $f(B)=2\sqrt{\frac{DB}{\kappa+B}}<2\sqrt{\frac{D}{\kappa+1}}\leq\hat{\rho}$ for $0<B<1$. Therefore, $\hat{\rho}^2\geq 4\frac{DB}{\kappa+B}$ so the relevant bounds on α are real, and thus, well-defined.

We now have a positively invariant triangular region in the phase plane with vertices of $(0,0)$, $(1,0)$, and $(0,\frac{\hat{\rho}}{2})$. A trajectory that leaves the saddle point, $(0,0)$ will do so tangent to the unstable eigenvector associated with the positive eigenvalue of the Jacobian matrix at $(0,0)$, given by

$$\mathbf{v}=\begin{pmatrix}1\\ \lambda^+\end{pmatrix},\ \text{where } \lambda^+=\frac{-\hat{\rho}+\sqrt{\hat{\rho}^2+\frac{4D}{\kappa}}}{2}.$$

Therefore, a trajectory leaving $(0,0)$ enters the trapping region. There are no periodic orbits within the region, since B increases monotonically while $V=B'>0$. Then, by the Poincaré-Bendixson theorem, a trajectory that enters the positively invariant region must converge to the equilibrium at $(1,0)$. Since the unstable manifold is one-dimensional, there is only one trajectory that originates from $(0,0)$ and enters the $B>0$, $V>0$ quadrant. Thus, we have established the existence of a unique monotone increasing wavefront, $B(z)$, satisfying the conditions,

$$\lim_{z\to-\infty}B(z)=0,\quad \lim_{z\to\infty}B(z)=1,\quad \text{and}\quad \lim_{z\to\pm\infty}B'(z)=0.$$

As previously discussed, this travelling wave moves along the positive z-axis. Physically speaking, this means that water with low BOD concentration invades water with high BOD concentration as the wave moves downstream, and so this travelling wave describes purification of the river. The phase portrait and travelling wave solution are shown numerically in Figure 3.2 for the case of specific parameter values. These waves are also observed when the BOD PDE, (1.4) is solved numerically, as presented in Figure 3.3.

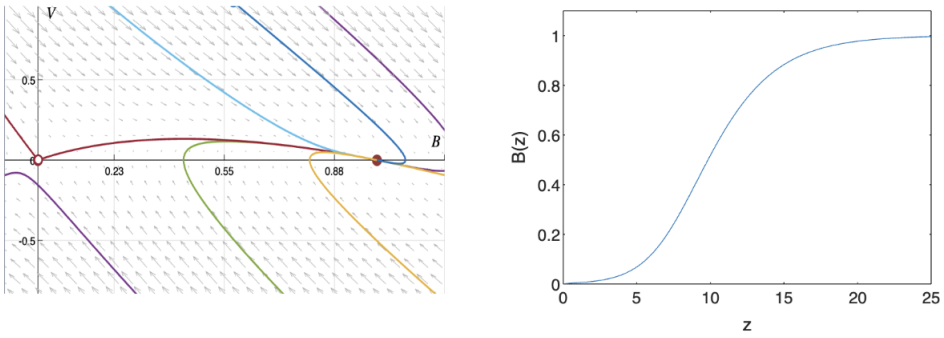

Figure 3.2. *Phase portrait (left) and numerical solution (right) of (2.1) with* $D = 1$, $\kappa = 0.5$, *and* $\hat{\rho} = 2.3$.

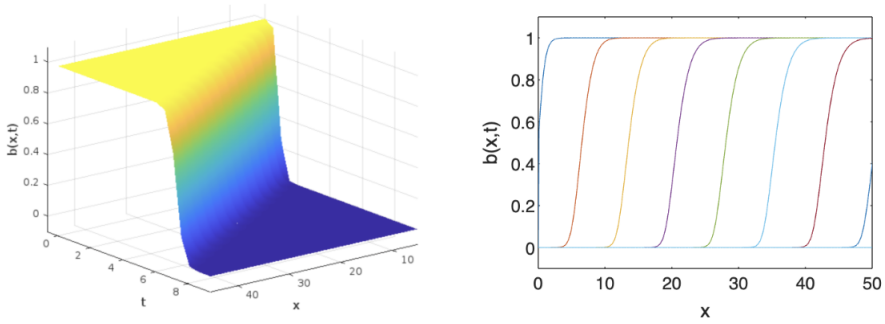

Figure 3.3. *Numerical solution of (1.4) when* $D = 1$, $P = 5$, $\kappa = 0.5$. *Boundary conditions of* $b(0,t) = 0$ *and* $b(50,t) = 1$ *were imposed, as well as an initial condition of* $u(x,0) = 0.5\tanh(x) + 0.5$. *A surface plot is shown in the left panel, and a plot of several waves with equidistant time steps is shown in the right panel.*

3.2. Case 2: $\hat{\rho} \leq -\rho^*$. When $\hat{\rho} \leq -\rho^*$, travelling waves, if they exist, travel sufficiently slower than the river. This case is similar to Case 1, only essentially reversed. We look for a trajectory that leaves the unstable node at $(1,0)$ and converges to the saddle point at $(0,0)$ along its stable manifold. The existence of this trajectory is shown by the construction of a negatively invariant trapping region with vertices $(0,0)$, $(1,0)$, and $(0,-\alpha)$ as shown in Figure 3.4. A similar argument was used in [5] as a general technique to show the existence of a heteroclinic orbit between an unstable node and a saddle point. Proceeding similarly as in Case 1, along $V = 0$ with $0 < B < 1$,

$$B' = 0,$$
$$V' = D\frac{B(1-B)}{\kappa + B} > 0$$

so trajectories point vertically upwards, and thus, out of the region. Along $B = 0$ with $V < 0$,

$$B' = V < 0,$$
$$V' = -\hat{\rho} < 0$$

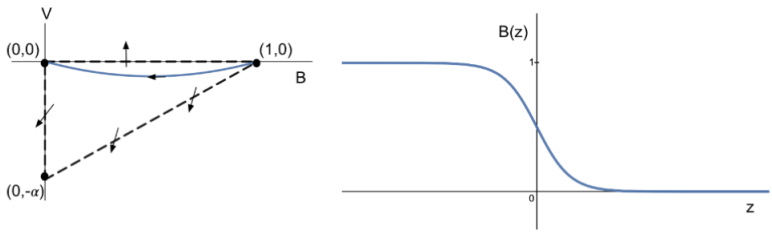

Figure 3.4. *Illustrations of a negatively invariant region enclosing a heteroclinic trajectory that connects* $(1,0)$ *to* $(0,0)$ *(left) and the corresponding travelling wave (right).*

so trajectories point downwards and to the right, leaving the region. Finally, along $V = \alpha(B-1)$ with $0 < B < 1$,

$$B' = \alpha(B-1) < 0,$$
$$V' = -\hat{\rho}\alpha(B-1) + D\frac{B(1-B)}{\kappa + B}$$

so trajectories point to the left. Using the arguments from Case 1, it can be shown that trajectories along $V = \alpha(B-1)$ point out of the trapping region if $\alpha = -\frac{\hat{\rho}}{2}$, so the triangular region defined by vertices $(0,0)$, $(1,0)$, and $(0, \frac{\hat{\rho}}{2})$ is negatively invariant. A trajectory converging to $(0,0)$ along its stable manifold must do so tangent to the eigenvector associated with the negative eigenvalue of the Jacobian matrix at $(0,0)$, given by

$$\mathbf{v} = \begin{pmatrix} 1 \\ \lambda^- \end{pmatrix}, \text{ where } \lambda^- = \frac{-\hat{\rho} - \sqrt{\hat{\rho}^2 + \frac{4D}{\kappa}}}{2}.$$

This eigenvector points to $(0,0)$ from the region, and thus, a trajectory tangent to it must have originated from somewhere in the region. Since there are no other equilibria or periodic orbits, the trajectory must have originated from the unstable node at $(1,0)$. By the arguments in Case 1, this trajectory is unique. So we have the existence of a unique monotone decreasing wavefront, $B(z)$ with the conditions

$$\lim_{z\to-\infty} B(z) = 1, \quad \lim_{z\to\infty} B(z) = 0, \quad \text{and} \quad \lim_{z\to\pm\infty} B'(z) = 0.$$

This wave describes contamination of the river, since water with high BOD concentration invades water with low BOD concentration as the wave travels downstream. The phase portrait and travelling wave solution for this case are shown in Figure 3.5 for certain parameter values. Figure 3.6 shows these waves as numerical solutions to the PDE, (1.4).

3.3. Case 3: $\hat{\rho} = 0$. In this case, waves travel at the same speed as the river. We have a saddle point at $(0,0)$ and centres at $(1,0)$. The existence of a heteroclinic orbit is clearly not possible in this case, so we instead look for a homoclinic orbit that originates along the unstable manifold of $(0,0)$ and asymptotically converges along the stable manifold of the

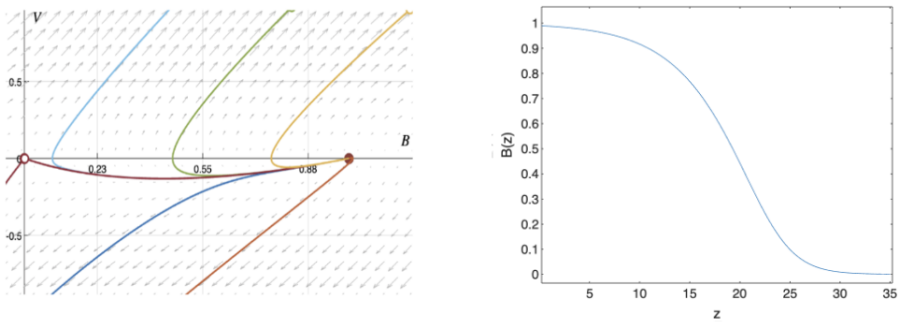

Figure 3.5. *Phase portrait (left) and numerical solution (right) of (2.1) with* $D = 1$, $\kappa = 0.5$, *and* $\hat{\rho} = -3.2$

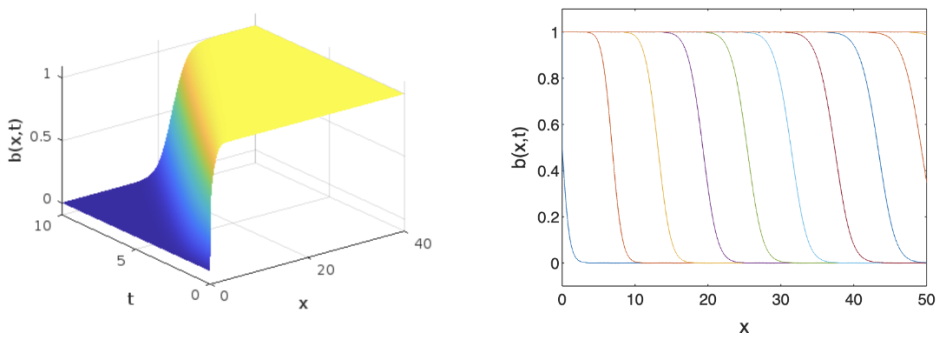

Figure 3.6. *Numerical solution of (1.4) when* $D = 1$, $P = 5$, $\kappa = 0.5$. *Boundary conditions of* $b(0,t) = 1$ *and* $b(50,t) = 0$ *were imposed, as well as an initial condition of* $u(x,0) = -0.5\tanh(x) + 0.5$. *A surface plot is shown in the left panel, and a plot with several curves with equidistant time steps are plotted in the right panel.*

saddle as $z \to \infty$. This trajectory corresponds to a travelling wave in the form of a pulse rather than a wavefront [7]. In this case, the BOD system is reduced to

$$\begin{aligned} B' &= V, \\ V' &= D\frac{B(1-B)}{\kappa + B} \end{aligned}$$

which is a conservative system. The trajectories of this system are equivalent to the level curves of an energy function given by $H(B,V)$, where

$$\frac{\partial H}{\partial V} = \frac{dB}{dz} \quad \text{and} \quad \frac{\partial H}{\partial B} = -\frac{dV}{dz}. \tag{3.5}$$

Notice

$$\frac{\partial H}{\partial B}\cdot\frac{dB}{dz} = -\frac{\partial H}{\partial V}\cdot\frac{dV}{dz} \implies \frac{\partial H}{\partial B}\cdot\frac{dB}{dz} + \frac{\partial H}{dV}\cdot\frac{dV}{dz} = 0 \implies \frac{dH}{dz} = 0$$

so $H(B,V)$ is constant with respect to z. Solving (3.5) and applying the boundary conditions, (2.3) results in an equation for the homoclinic orbit in the phase plane,

$$V^2 = -D\left[B^2 + 2(\kappa+1)\left(\kappa \ln\left(\frac{B+\kappa}{\kappa}\right) - B\right)\right].$$

The existence of this trajectory implies the existence of a unique travelling wave solution in the form of a pulse to (1.4). This wave describes temporary contamination followed by purification as it travels down the river. The phase portrait and pulse solution are shown in Figure 3.7.

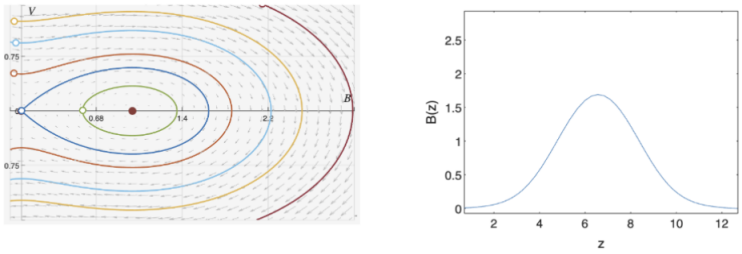

Figure 3.7. *Phase portrait (left) and numerical solution (right) of (2.1) with* $D = 1$, $\kappa = 0.5$, *and* $\hat{\rho} = 0$.

3.4. Cases 4 and 5: $0 < |\hat{\rho}| < \rho^*$. When the speed of the wave is sufficiently close to the speed of the river, $(1,0)$ is a spiral in the phase plane and we end up with wavefronts that oscillate indefinitely about the horizontal line, $B(z) = 1$. These types of solutions have not been well studied in similar models, and are often rejected on the basis of physical irrelevance. This is because the range of the oscillatory solutions can exceed the intended bounds on solutions to a problem.

For example, in the case of the F-KPP equation which is a population model, travelling wave solutions with dimensionless speeds of less than 2 are rejected on the basis of physical and mathematical irrelevance. In the physical sense, oscillations force these solutions to be negative at times [13], which is nonsensical in terms of populations. Additionally, [8] proves the instability of these non-monotone travelling wave solutions which mathematically supports their rejection.

In our model, solutions that oscillate around the dimensionless BOD saturation level, $b(x,t) = 1$ are still physically meaningful. The existence of these solutions has been difficult to prove analytically, so we give here an intuitive argument based on phase portraits and numerical solutions of (2.1). In the case where $0 < \hat{\rho} < \rho^*$, we have a stable spiral at $(1,0)$ so we are interested in a trajectory that connects $(0,0)$ to $(1,0)$. Based on the phase portrait, a trajectory originating at $(0,0)$ converges to $(1,0)$ while oscillating around it. Conversely, when $0 > \hat{\rho} > -\rho^*$, $(1,0)$ is an unstable spiral, so a trajectory that converges to $(0,0)$ would have originated from $(1,0)$ while oscillating around it. Phase portraits in these cases are shown in Figure 3.8 and strongly suggest the existence of a trajectory that connects the two equilibria. These trajectories result in oscillatory travelling wave solutions, as shown in Figure 3.9. The cases of the stable and unstable spirals result in purification and contamination waves, respectively, following from the arguments used in Cases 1 and 2.

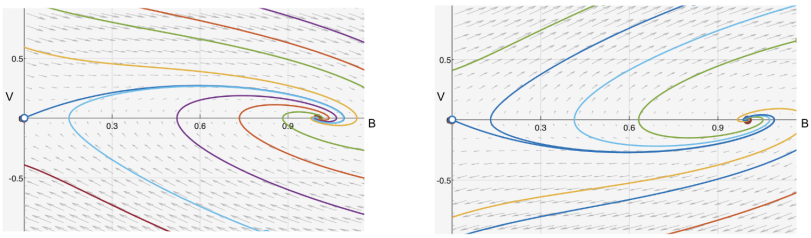

Figure 3.8. *Phase portraits for the case of a stable spiral at* $(1,0)$ *(left) where* $D=1$, $\kappa=0.5$, $\hat{\rho}=-0.8165$ *and unstable spiral at* $(1,0)$ *(right) where* $D=1$, $\kappa=0.5$, $\hat{\rho}=0.8165$.

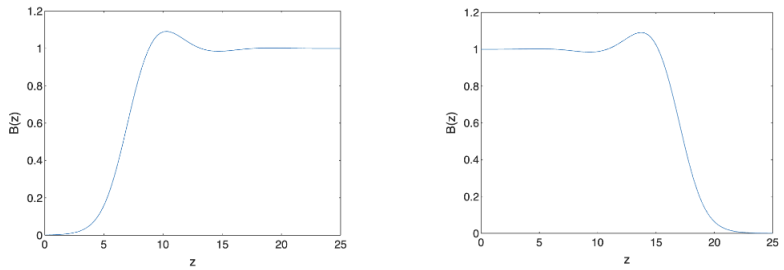

Figure 3.9. *Non-monotone travelling wave solutions to (2.1) where* $D=1$, $\kappa=0.5$, $\hat{\rho}=-0.8165$ *(left) and* $\hat{\rho}=0.8165$ *(right).*

4. Solution to the Dissolved Oxygen Equation. Since we now know that solutions to (2.1) exist and satisfy (2.3) for all values of $\hat{\rho}$, we can solve the travelling wave equation for DO, (2.2) in terms of $B(z)$, subject to the conditions, (2.4). Equation (2.2) was given by

$$C''+\hat{\rho}C'-SC=\hat{D}g(B)-S.$$

By assuming an exponential solution form of $C_h(z)=e^{rz}$ (where r is an unknown constant) to the homogeneous problem and using the method of variation of parameters to obtain a particular solution, we obtain a general solution to (2.2) of

$$C(z)=a_1e^{r_1z}+a_2e^{r_2z}+\frac{e^{r_2z}}{r_2-r_1}\int\frac{\hat{D}g(B(z))}{e^{r_2z}}dz-\frac{e^{r_1z}}{r_2-r_1}\int\frac{\hat{D}g(B(z))}{e^{r_1z}}dz+1 \tag{4.1}$$

where a_1, a_2 are integration constants, and $r_1=\frac{-\hat{\rho}+\sqrt{\hat{\rho}^2+4S}}{2}>0$, $r_2=\frac{-\hat{\rho}-\sqrt{\hat{\rho}^2+4S}}{2}<0$ are the roots of the characteristic polynomial of (2.2).

The integration constants associated with the integrals in (4.1) are chosen in a way that results in

$$C(z)=a_1e^{r_1z}+a_2e^{r_2z}+\frac{e^{r_2z}}{r_2-r_1}\int_{-\infty}^{z}\frac{\hat{D}g(B(s))}{e^{r_2s}}ds-\frac{e^{r_1z}}{r_2-r_1}\int_{\infty}^{z}\frac{\hat{D}g(B(s))}{e^{r_1s}}ds+1.$$

Taking the limit as $z \to \infty$ of $C(z)$ results in $a_2 e^{r_2 z} \to 0$ since $r_2 < 0$. Also,

$$\lim_{z\to\infty} \frac{e^{r_1 z}}{r_2 - r_1} \int_{\infty}^{z} \frac{\hat{D}g(B(s))}{e^{r_1 s}} ds = \frac{1}{r_2 - r_1} \lim_{z\to\infty} \frac{\int_{\infty}^{z} \frac{\hat{D}g(B(s))}{e^{r_1 s}} ds}{e^{-r_1 z}}.$$

By l'Hôpital's rule and the Fundamental Theorem of Calculus, this expression is equivalent to

$$\frac{1}{r_2 - r_1} \lim_{z\to\infty} \frac{\hat{D}g(B(z))e^{-r_1 z}}{-r_1 e^{-r_1 z}} = \frac{1}{r_2 - r_1} \lim_{z\to\infty} \frac{-\hat{D}g(B(z))}{r_1} = 0$$

by (2.3). Thus, we have

$$\lim_{z\to\infty} C(z) = \lim_{z\to\infty} \left(a_1 e^{r_1 z} + \frac{e^{r_2 z}}{r_2 - r_1} \int_{-\infty}^{z} \frac{\hat{D}g(B(s))}{e^{r_2 s}} ds + 1 \right).$$

Now,

$$\begin{aligned} \left| \lim_{z\to\infty} \frac{e^{r_2 z}}{r_2 - r_1} \int_{-\infty}^{z} \frac{\hat{D}g(B(s))}{e^{r_2 s}} ds \right| &\leq \lim_{z\to\infty} \frac{\hat{D}||g(B)||_\infty e^{r_2 z}}{|r_2 - r_1|} \int_{-\infty}^{z} e^{-r_2 s} ds \\ = \lim_{z\to\infty} \frac{\hat{D}||g(B)||_\infty e^{r_2 z}}{|r_2 - r_1|} \left(-\frac{1}{r_2} e^{-r_2 z} + \frac{1}{r_2} e^{r_2(\infty)} \right) &= \frac{\hat{D}||g(B)||_\infty}{r_2(r_2 - r_1)} \end{aligned}$$

where $||g(B)||_\infty$ is the supremum of $|g(B(z))|$ over z. We then define

$$l := \lim_{z\to\infty} \frac{e^{r_2 z}}{r_2 - r_1} \int_{-\infty}^{z} \frac{\hat{D}g(B(s))}{e^{r_2 s}} ds \in \left[-\frac{\hat{D}||g(B)||_\infty}{r_2(r_2 - r_1)}, \frac{\hat{D}||g(B)||_\infty}{r_2(r_2 - r_1)} \right] \tag{4.2}$$

so l is a finite constant. Therefore, applying the right-sided boundary condition, $\lim_{z\to\infty} C(z) = 1$ from (2.4) gives

$$\lim_{z\to\infty} C(z) = \lim_{z\to\infty} a_1 e^{r_1 z} + l = 0 \implies a_1 = \frac{-l}{\lim_{z\to\infty} e^{r_1 z}}.$$

Since $\lim_{z\to\infty} e^{r_1 z} = \infty$ and l is a finite constant, this implies that a_1 must be zero for the boundary condition to hold. By the same reasoning, it can be shown that implementing the left-sided boundary condition, $\lim_{z\to-\infty} C(z) = 1$ implies $a_2 = 0$. Therefore,

$$C(z) = \frac{e^{r_2 z}}{r_2 - r_1} \int_{-\infty}^{z} \frac{\hat{D}g(B(s))}{e^{r_2 s}} ds - \frac{e^{r_1 z}}{r_2 - r_1} \int_{-\infty}^{z} \frac{\hat{D}g(B(s))}{e^{r_1 s}} ds + 1. \tag{4.3}$$

and we have

$$\begin{aligned} \lim_{z\to\infty} C(z) &= \lim_{z\to\infty} \left(\frac{e^{r_2 z}}{r_2 - r_1} \int_{-\infty}^{z} \frac{\hat{D}g(B(s))}{e^{r_2 s}} ds - \frac{e^{r_1 z}}{r_2 - r_1} \int_{\infty}^{z} \frac{\hat{D}g(B(s))}{e^{r_1 s}} ds + 1 \right) \\ &= l - 0 + 1. \end{aligned}$$

Now, we know that $C(z)$ converges to a finite constant as $z \to \pm\infty$. To verify that this constant is 1 (i.e. $\lim_{z\to\pm\infty} C(z) = 1$), consider

$$\bar{C}'' + \hat{\rho}\bar{C}' = S(1 - \bar{C}) \tag{4.4}$$

which is equivalent to (2.2) for $z \to \pm\infty$ since we know $g(B(z)) \to 0$. The only constant solution of (4.4) is $\bar{C}(z) = 1$ so $C(z) \to 1$ as $z \to \infty$. Therefore, $\lim_{z\to\infty} C(z) = 1$ and so it follows that $l + 1 = 1$, and thus, $l = 0$. Now, differentiating (4.3) with respect to z results in

$$\begin{aligned}\lim_{z\to\infty} C'(z) &= \lim_{z\to\infty} \left(\frac{r_2 e^{r_2 z}}{r_2 - r_1} \int_{-\infty}^{z} \frac{\hat{D}g(B(s))}{e^{r_2 s}} ds - \frac{r_1 e^{r_1 z}}{r_2 - r_1} \int_{\infty}^{z} \frac{\hat{D}g(B(s))}{e^{r_1 s}} ds \right) \\ &= r_2 l + 0 = 0.\end{aligned}$$

The same argument can be made to show that $\lim_{z\to-\infty} C(z) = 1$ and $\lim_{z\to-\infty} C'(z) = 0$. Therefore, we conclude that a solution exists to (2.2) and (2.4) whenever a solution to (2.1) exists that satisfies (2.3).

Thus, we have shown that travelling wave solutions exist to (1.4) and (1.5) for any wave speed, although not all of these are stable, as will be discussed in section 5. Figure 4.1 shows the pulse-type travelling wave solution to (1.5) when solved numerically. This solution agrees with the DO sag curve as depicted in Figure 1.1.

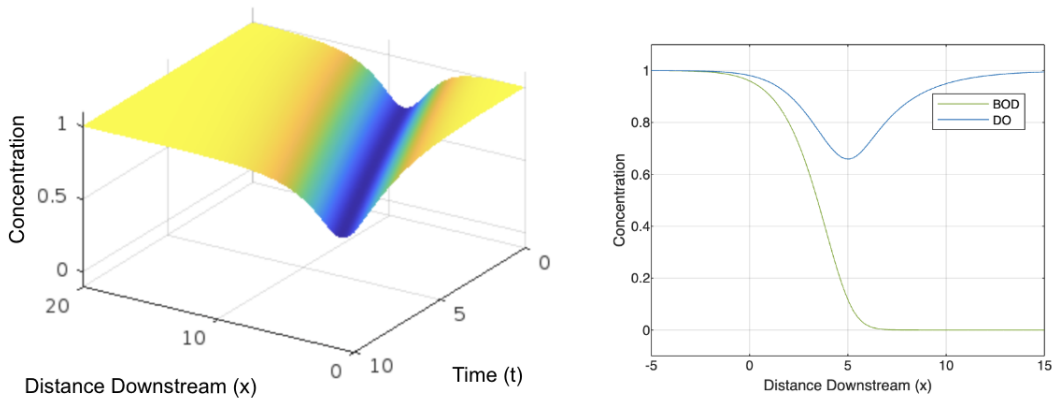

Figure 4.1. *Numerical solution to (1.5). A surface plot is depicted on the left, and the solution at $t = 5$ is shown in the $b - x$ plane on the right. Parameter values of $D = 1$, $\hat{D} = 1$, $P = 1$, $\kappa = 0.1$, and $S = 1$ were implemented.*

5. Stability of Travelling Waves.

Now that the existence of travelling waves has been established, the next question we have to address is their stability. We start with the case of monotone waves (Cases 1 and 2) and show the spectral stability of solutions to (1.4) and (1.5) by imposing perturbations to travelling wave solutions of each PDE and showing that the perturbations die out as $t \to \infty$. This method is commonly used to show spectral stability, and is demonstrated in [7] and [13] for the F-KPP equation.

To start, we assume solutions to (1.4) and (1.5) of $b(x,t) := b(z,t)$ and $c(x,t) := c(z,t)$, respectively, where $z = x - \rho t$. Substituting $b(z,t)$ into (1.4) and $c(z,t)$ into (1.5) gives

$$Lb := \frac{\partial b}{\partial t} - \frac{\partial^2 b}{\partial z^2} - \hat{\rho}\frac{\partial b}{\partial z} = -Dg(b) \tag{5.1}$$

$$Lc := \frac{\partial c}{\partial t} - \frac{\partial^2 c}{\partial z^2} - \hat{\rho}\frac{\partial c}{\partial z} = -\hat{D}g(b) + S(1-c). \tag{5.2}$$

We then define $b(z,t) := B(z) + v_1(z,t)$ and $c(z,t) := C(z) + v_2(z,t)$ where $B(z)$ and $C(z)$ are travelling wave solutions to their respective PDEs. Also, $v_1(z,t)$ and $v_2(z,t)$ are small perturbations, where $0 < |v_i(z,t)| << 1$ and $\lim_{z\to\pm\infty} v_i(z,t) = 0$ for $i = 1, 2$. Substituting $b(z,t)$ and $c(z,t)$ into (5.1) and (5.2) gives

$$LB + Lv_1 = -Dg(B) - Dg(B + v_1) + Dg(B) \tag{5.3}$$

$$LC + Lv_2 = -\hat{D}g(B) - \hat{D}g(B + v_2) + \hat{D}g(B) + S(1 - C - v_2). \tag{5.4}$$

Since $B(z)$ and $C(z)$ satisfy (2.1), (2.2) and do not depend on t, (5.3) and (5.4) simplify to

$$Lv_1 = D\left(g(B) - g(B + v_1)\right) \tag{5.5}$$

$$Lv_2 = \hat{D}\left(g(B) - g(B + v_2)\right) - Sv_2. \tag{5.6}$$

We linearize g to obtain $g(B+v_i) = g(B) + g'(B)v_i + \mathcal{O}(v_i^2)$ and since v_i is small, $g(B+v_i) \approx g(B) + g'(B)v_i$ for $i = 1, 2$. Then,

$$Lv_1 \approx -Dg'(B)v_1$$
$$Lv_2 \approx -\hat{D}g'(B)v_2 - Sv_2.$$

By assuming a separation of variables ansatz, $v_1(z,t) = y_1(z)f_1(t)$ and $v_2(z,t) = y_2(z)f_2(t)$, two separate ODEs are obtained for each equation, given by

$$y_1'' + \hat{\rho}y_1' + (\lambda_1 - Dg'(B))y_1 = 0, \tag{5.7}$$

$$f_1' + \lambda_1 f_1 = 0 \tag{5.8}$$

and

$$y_2'' + \hat{\rho}y_2' + (\lambda_2 - \hat{D}g'(B) - S)y_2 = 0, \tag{5.9}$$

$$f_2' + \lambda_2 f_2 = 0 \tag{5.10}$$

where λ_1 and λ_2 are eigenvalues with corresponding eigenfunctions, $y_1 = y_1(z)$ and $y_2 = y_2(z)$. Equations (5.8) and (5.10) are solved to obtain $f_1(t) = c_1 e^{-\lambda_1 t}$ and $f_2(t) = c_2 e^{-\lambda_2 t}$ where c_1 and c_2 are integration constants. Then, $v_1(z,t) = y_1(z)e^{-\lambda_1 t}$ and $v_2(z,t) = y_2(z)e^{-\lambda_2 t}$. To determine the signs of λ_1 and λ_2, the Liouville-Green transformations, $y_1(z) = h_1(z)e^{-\hat{\rho}z/2}$, and $y_2(z) = h_2(z)e^{-\hat{\rho}z/2}$ are applied in (5.7) and (5.9) to obtain

$$-h_1'' + \left(Dg'(B) + \frac{\hat{\rho}^2}{4}\right)h_1 = \lambda_1 h_1 \tag{5.11}$$

$$. - h_2'' + \left(\hat{D}g'(B) + S + \frac{\hat{\rho}^2}{4}\right)h_2 = \lambda_2 h_2. \tag{5.12}$$

Then, by the Rayleigh quotient,

$$\lambda_1 = \frac{\int_{-\infty}^{\infty} h_1'^2 + \left(Dg'(B) + \frac{\hat{\rho}^2}{4}\right) h_1^2 dz - h_1 h_1'\Big|_{-\infty}^{\infty}}{||h_1||^2} \tag{5.13}$$

$$= \frac{\int_{-\infty}^{\infty} h_1'^2 + \left(Dg'(B) + \frac{\hat{\rho}^2}{4}\right) h_1^2 dz}{||h_1||^2}$$

$$\lambda_2 = \frac{\int_{-\infty}^{\infty} h_2'^2 + \left(\hat{D}g'(B) + S + \frac{\hat{\rho}^2}{4}\right) h_2^2 dz - h_2 h_2'\Big|_{-\infty}^{\infty}}{||h_2||^2} \tag{5.14}$$

$$= \frac{\int_{-\infty}^{\infty} h_2'^2 + \left(Dg'(B) + \frac{\hat{\rho}^2}{4}\right) h_2^2 dz}{||h_2||^2}$$

since $v(z,t) \to 0 \implies h(z,t) \to 0$ as $z \to \pm\infty$. In the case of monotone waves, we have $\hat{\rho}^2 \geq \frac{4D}{\kappa+1}$, so

$$Dg'(B) + \frac{\hat{\rho}^2}{4} \geq D\left(g'(B) + \frac{1}{\kappa+1}\right) = D\left(\frac{-B^2 - 2\kappa B + \kappa}{(\kappa+B)^2} + \frac{1}{\kappa+1}\right).$$

Since $B < 1$ in this case,

$$Dg'(B) + \frac{\hat{\rho}^2}{4} \geq D\left(\frac{-B^2 - 2\kappa B + 2\kappa + B}{(\kappa+B)^2}\right) = D\frac{(1-B)(2\kappa+B)}{(\kappa+B)^2} > 0.$$

Similarly,

$$\hat{D}g'(B) + S + \frac{\hat{\rho}^2}{4} \geq D\left(\frac{b_s}{c_s} \cdot \frac{(1-B)(2\kappa+B)}{(\kappa+B)^2}\right) + S > 0.$$

Therefore, from (5.13) and (5.14), $\lambda_1 > 0$ for each $h_1(z)$ and $\lambda_2 > 0$ for each $h_2(z)$, so the problems (5.11) and (5.12) have only positive eigenvalues. Thus, $v_1(z,t) = y_1(z)e^{-\lambda_1 t} \to 0$ and $v_2(z,t) = y_2(z)e^{-\lambda_2 t} \to 0$ as $t \to \infty$. This means that sufficiently small perturbations to initial conditions in (1.4) and (1.5) will die out, and the solutions, $b(z,t)$ and $c(z,t)$ converge to the travelling waves, $B(z)$ and $C(z)$ as $t \to \infty$. This implies the spectral stability of travelling wave solutions to (1.4) and (1.5) when $|\hat{\rho}| \geq \rho^*$ (Cases 1 and 2).

Conversely, the non-monotone wave solutions to (1.4) that occur when $|\hat{\rho}| < \rho^*$ (as in Cases 3, 4 and 5) are unstable. This result follows directly from [8] who proved the instability of a large class of non-monotone travelling waves. Therefore, travelling wave solutions to (1.5) are also unstable for $|\hat{\rho}| < \rho^*$.

6. Approximate Solution of Monotone Travelling Waves. In this section, we obtain an approximation of the monotone wavefront solution to (2.1) by a perturbation method. This method is demonstrated in [11] and [13], for example. The idea is to determine an approximate

travelling wave solution in the form of a power series in some small parameter, ϵ. We begin by defining $\epsilon := \frac{D}{\hat{\rho}^2}$. In the case of the monotone wavefronts, we have $\hat{\rho}^2 > \frac{4D}{\kappa+1}$ so it follows that $\epsilon = \frac{D}{\hat{\rho}^2} \leq \frac{\kappa+1}{4} < \frac{1}{2}$ since $0 < \kappa < 1$. Substituting ϵ into (2.1), we obtain

$$\sqrt{\frac{\epsilon}{D}}B''(z) + B'(z) - \sqrt{\frac{\epsilon}{D}}Dg(B(z)) = 0.$$

Making the change of variables $s := \sqrt{\frac{\epsilon}{D}}z$ and $f(s) := B\left(\sqrt{\frac{D}{\epsilon}}s\right)$ results in

$$\epsilon f''(s) + Df'(s) - D^2 g(f(s)) = 0. \tag{6.1}$$

We then write $f(s)$ as a power series in terms of ϵ,

$$f(s) = f_0(s) + \epsilon f_1(s) + \epsilon^2 f_2(s) + ...$$

and substitute into (6.1),

$$\epsilon(f_0'' + \epsilon f_1'' + \epsilon^2 f_2'' + ...) + D(f_0' + \epsilon f_1' + \epsilon^2 f_2' + ...) - D^2 g(f_0 + \epsilon f_1 + \epsilon^2 f_2 + ...) = 0. \tag{6.2}$$

Grouping by powers of ϵ and linearizing the last term, (6.2) becomes

$$Df_0' - D^2 g(f_0) + \epsilon\left(f_0'' + Df_1' - D^2 g'(f_1)\right) + \epsilon^2\left(f_1'' + Df_2' - D^2 g''(f_2)\right) + ... \approx 0$$

and thus

$$Df_0' - D^2 g(f_0) + \mathcal{O}(\epsilon) \approx 0. \tag{6.3}$$

Since $\epsilon < \frac{1}{2}$, (6.3) can be approximated by

$$f_0'(s) = Dg(f_0(s)), \quad f(0) = \frac{1}{2}$$

when $\epsilon \to 0$. The boundary condition is imposed for convenience without loss of generality, since any travelling wave solution can be scaled by a horizontal shift along the z-axis. Equation (6.1) is separable, and is solved to obtain an implicit equation for $f_0(s)$ as

$$\frac{(1 - f_0(s))^{\kappa+1}}{f_0(s)^\kappa} \approx \tfrac{1}{2}e^{-Ds} \tag{6.4}$$

once the boundary condition is imposed. In the case of simpler expressions, one would then use the result obtained for $f_0(s)$ to solve sequentially for $f_1(s)$ when $\epsilon^2 \to 0$, $f_2(s)$ when $\epsilon^3 \to 0$, and so on, resulting in increasingly more accurate approximations of $f(s)$. However, due to the implicit form of (6.4), solving for higher order terms becomes very difficult, so here, we obtain only a first order approximation of $f(s)$ with an error of $\mathcal{O}\left(\frac{D}{\hat{\rho}^2}\right)$ where $\frac{D}{\hat{\rho}^2} < \frac{1}{2}$. This approximation is given by

$$\frac{(1 - f(s))^{\kappa+1}}{f(s)^\kappa} \approx \tfrac{1}{2}e^{-Ds}.$$

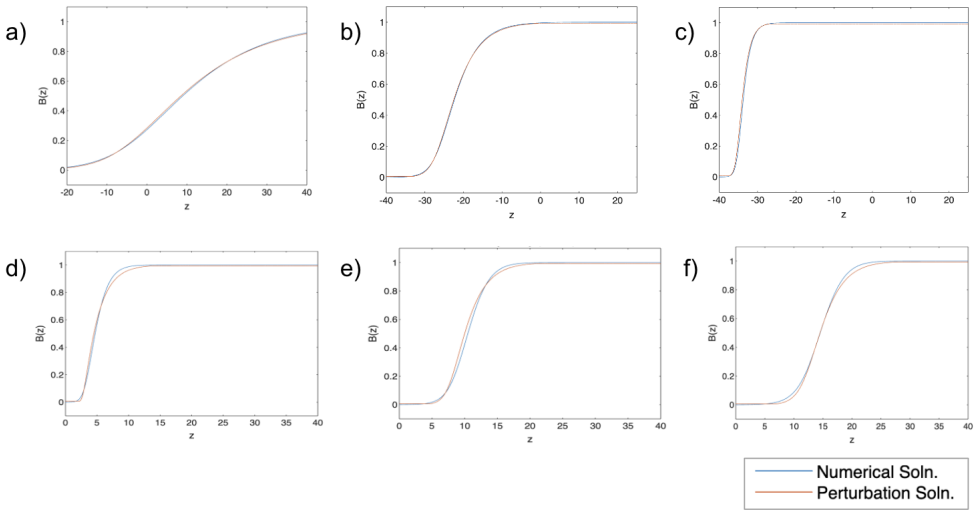

Figure 6.1. *Numerical solution (blue) and perturbation solution (orange) of (2.1). For a), b) and c), $\kappa = 0.5$ and $\hat{\rho} = 2\rho^*$. $D = 0.1$ in a), $D = 1$ in b), and $D = 10$ in c). For d), e) and f), $D = 1$ and $\hat{\rho} = \rho^*$. $\kappa = 0.1$ in d), $\kappa = 0.5$ in e) and $\kappa = 0.9$ in f).*

so an approximation for the monotone travelling wavefront, $B(z)$ is

$$\frac{(1 - B(z))^{\kappa+1}}{B(z)^{\kappa}} \approx \tfrac{1}{2} e^{-\frac{D}{\hat{\rho}} z}. \tag{6.5}$$

This equation also allows us to estimate the slope of the wave for different wave speeds. Differentiating both sides of (6.5) and solving for $B'(z)$ results in

$$B'(z) \approx \frac{DB(1 - B)}{\hat{\rho}(B + \kappa)}$$

and so we observe that the closer the wave travels to the speed of the river, the steeper its slope. Figure 6.1 compares the analytical approximation obtained from the perturbation method with the numerical solution to (2.1) under the same set of parameter values. It is seen from both the analysis and numerics that the approximation, (6.5) is more accurate for $|\hat{\rho}| \gg \rho^*$ but is still a decent representation of the solution for any value of $\hat{\rho}$ where $|\hat{\rho}| \gtrsim \rho^*$. An approximation for the travelling wave solution, $C(z)$ to (1.5) could be obtained by substituting the approximation for $B(z)$ into (4.3), but due to the implicit form of (6.5), this would not give an analytical equation.

7. Discussion and Conclusion.

7.1. Summary of Results. We have shown that travelling waves exist to (1.4) as purification waves when travelling faster than the river and as contamination waves when travelling slower than the river. Furthermore, these waves must travel sufficiently faster or slower than the river in order to be stable, as waves travelling close to the speed of the river are unstable.

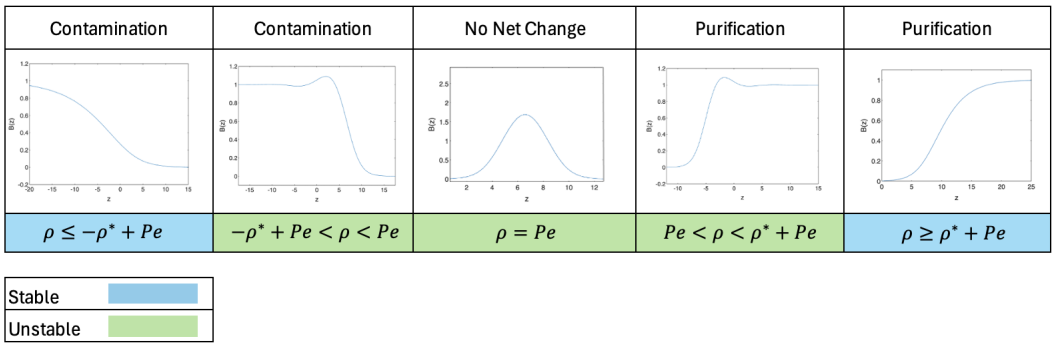

Figure 7.1. *Summary of the travelling wave solutions to (1.4) for a given speed, ρ.*

The speed, classification, and stability of the different types of waves is summarized in Figure 7.1. We also showed that a spectrally stable travelling wave solution to the linear equation, (1.5) exists for all wave speeds and resembles the dissolved oxygen sag curve as depicted in Figure 1.1.

7.2. Connection to the Generalized Fisher-KPP Equation. Here, we briefly discuss the relationship between the BOD equation, (1.4) and the widely studied generalized F-KPP equation given in dimensionless form,

$$\frac{\partial u}{\partial t} = \frac{\partial^2 u}{\partial x^2} + f(u) \tag{7.1}$$

where $f(u)$ satisfies

$$f(0) = f(m) = 0, \quad f'(0) > 0, \quad f'(m) < 0, \quad \text{and} \quad f''(u) < 0 \tag{7.2}$$

for some $m \in \mathbb{R}$. The existence of travelling wave solutions to (7.1) is known [9], [1], [17], [3]. The asymptotic stability of the travelling waves is also well established [17], [14], [18].

Under the change of variables, $(x, t) \to (\bar{x} := x - P \cdot t, \bar{t})$, equation (1.4) becomes

$$\frac{\partial b}{\partial \bar{t}} = \frac{\partial^2 b}{\partial \bar{x}^2} - D\frac{b(1-b)}{\kappa + b}. \tag{7.3}$$

Then, with the transformation, $b = 1 - \bar{b}$, (7.3) becomes

$$\frac{\partial \bar{b}}{\partial \bar{t}} = \frac{\partial^2 \bar{b}}{\partial \bar{x}^2} + D\frac{\bar{b}(1-\bar{b})}{\kappa - \bar{b} + 1}. \tag{7.4}$$

Taking $f(b) := D\frac{\bar{b}(1-\bar{b})}{\kappa - \bar{b}+1}$, the conditions, (7.2) hold for $\bar{b} \in [0, 1]$ with $m = 1$. Then, the existence and stability of travelling wave solutions to (7.4) that asymptotically connect the equilibria at $\bar{b} = 1$ and $\bar{b} = 0$ is guaranteed. This result implies the existence of travelling waves to (1.4) but with opposite orientation due to the transformation on b. In other words, wavefront solutions of (7.4) that connect $\bar{b} = 1$ to $\bar{b} = 0$ correspond to solutions of (1.4) that connect $b = 0$ to $b = 1$.

The advection term as well as the opposite orientation of solutions and added complexity of the non-linearity in (1.4) required modification of the usual analysis on the F-KPP equation. For example, the advection term leads to two additional cases to consider when studying the existence of travelling waves in section 3. Additionally, due to the sign of the non-linear term, we were not able to outwardly reject the existence of oscillatory travelling waves that occur when $0 < |\hat{\rho}| < \rho^*$ since these oscillations never force the solution to become negative as they do in the case of the F-KPP equation. Finally, because of the slightly more involved non-linear term in (1.4), in section 6, we were only able to obtain a first-order approximation of travelling wave solutions given in implicit form. In the case of the F-KPP equation, an approximation of at least second order can be obtained fairly easily, as demonstrated, for example, in [11].

7.3. Travelling Waves to the DO Equation. While the analysis behind the travelling wave solutions to (1.4) is based on well studied techniques, the existence of travelling wave solutions to (1.5) is an interesting result that makes this paper distinct. Travelling waves are not a common topic of study in river quality modelling, since traditional linear models such as (1.1), (1.2) do not give rise to such solutions. The travelling waves solutions of the linear DO equation, (1.5) only result as a consequence of the coupling to the non-linear BOD equation, (1.4) and are entirely driven by the travelling wave solutions of (1.4). Additionally, travelling waves in systems of PDEs are often difficult to study. In our case, the one-way coupling of (1.4) and (1.5) simplifies the analysis, allowing us to study the equations separately.

7.4. Future Work. Further work could be done to establish a relationship between initial conditions and wave speed, so that one could automatically determine the types of travelling waves permitted to the BOD equation, (1.4) based on initial data. In the case of the F-KPP equation, for example, it was first proven by [9] with later work done by [1] that initial data with compact support permits waves travelling at a dimensionless speed of 2. It would be interesting to determine if a similar result can be obtained for this model. Another possibility for future work is to add a coupled ODE to the PDE system, (1.4) and (1.5), modelling a microorganism population in the river that feeds on an organic pollutant, and investigate whether travelling waves are still permitted.

Appendix A. Dimensional Analysis. Here, we derive the dimensionless system given by (1.4) and (1.5). We start with the dimensional system, (1.1) and (1.2) but with the linear BOD decay term replaced by the Braun-Berthouex [2] decay term. We have

$$\frac{\partial b}{\partial t} + v\frac{\partial b}{\partial x} = K\frac{\partial^2 b}{\partial x^2} - \frac{\mu b(b_s - b)}{k_m + b} \tag{A.1}$$

$$\frac{\partial c}{\partial t} + v\frac{\partial c}{\partial x} = K\frac{\partial^2 c}{\partial x^2} - \frac{\mu b(b_s - b)}{k_m + b} + k_c(c_s - c) \tag{A.2}$$

where μ represents the growth rate of a microorganism population feeding on BOD, b_s is the BOD concentration saturation level, k_m is the BOD half-saturation constant, and k_c is the DO reaeration rate constant. We define dimensionless variables,

$$\tilde{B} = \frac{b}{b^*}, \quad \tilde{C} = \frac{c}{c^*}, \quad \tilde{X} = \frac{x}{x^*}, \quad \text{and} \quad \tilde{T} = \frac{t}{t^*} \tag{A.3}$$

where b^*, c^*, x^*, and t^* have the same dimensions as b, c, x, and t, respectively and will be determined later on. Substituting (A.3) into (A.1) and (A.2) results in

$$\frac{b^*}{t^*}\frac{\partial \tilde{B}}{\partial \tilde{T}} + v\frac{b^*}{x^*}\frac{\partial \tilde{B}}{\partial \tilde{X}} = K\frac{b^*}{(x^*)^2}\frac{\partial^2 \tilde{B}}{\partial \tilde{X}^2} - \frac{\mu b^* \tilde{B}(b_s - b^*\tilde{B})}{k_m + b^*\tilde{B}} \tag{A.4}$$

$$\frac{c^*}{t^*}\frac{\partial \tilde{C}}{\partial \tilde{T}} + v\frac{c^*}{x^*}\frac{\partial \tilde{C}}{\partial \tilde{X}} = K\frac{c^*}{(x^*)^2}\frac{\partial^2 \tilde{C}}{\partial \tilde{X}^2} - \frac{\mu b^* \tilde{B}(b_s - b^*\tilde{B})}{k_m + b^*\tilde{B}} + k_c(c_s - c^*\tilde{C}). \tag{A.5}$$

Multiplying (A.4) by $\frac{t^*}{b^*}$ and (A.5) by $\frac{t^*}{c^*}$ results in

$$\frac{\partial \tilde{B}}{\partial \tilde{T}} + v\frac{t^*}{x^*}\frac{\partial \tilde{B}}{\partial \tilde{X}} = K\frac{t^*}{(x^*)^2}\frac{\partial^2 \tilde{B}}{\partial \tilde{X}^2} - \frac{t^*}{b^*}\frac{\mu b^* \tilde{B}(b_s - b^*\tilde{B})}{k_m + b^*\tilde{B}}$$

$$\frac{\partial \tilde{C}}{\partial \tilde{T}} + v\frac{t^*}{x^*}\frac{\partial \tilde{C}}{\partial \tilde{X}} = K\frac{t^*}{(x^*)^2}\frac{\partial^2 \tilde{C}}{\partial \tilde{X}^2} - \frac{t^*}{c^*}\frac{\mu b^* \tilde{B}(b_s - b^*\tilde{B})}{k_m + b^*\tilde{B}} + k_c\frac{t^*}{c^*}(c_s - c^*\tilde{C}).$$

We define $x^* = L$ where L is a measure of length, $t^* = \frac{L^2}{D}$, $b^* = b_s$, and $c^* = c_s$ to obtain

$$\frac{\partial \tilde{B}}{\partial \tilde{T}} + \frac{vL}{K}\frac{\partial \tilde{B}}{\partial \tilde{X}} = \frac{\partial^2 \tilde{B}}{\partial \tilde{X}^2} - \frac{\mu L^2}{K}\frac{\tilde{B}(1-\tilde{B})}{\frac{k_m}{b_s} + \tilde{B}}$$

$$\frac{\partial \tilde{C}}{\partial \tilde{T}} + \frac{vL}{K}\frac{\partial \tilde{C}}{\partial \tilde{X}} = \frac{\partial^2 \tilde{C}}{\partial \tilde{X}^2} - \frac{b_s}{c_s}\frac{\mu L^2}{K}\frac{\tilde{B}(1-\tilde{B})}{\frac{k_m}{b_s} + \tilde{B}} + \frac{k_c L^2}{K}(1-\tilde{C}).$$

We choose $P = \frac{vL}{K}$, $D = \frac{\mu L^2}{K}$, $\hat{D} = \frac{b_s}{c_s}\frac{\mu L^2}{K}$, $S = \frac{k_c L^2}{K}$, and $\kappa = \frac{k_m}{b_s}$. Then,

$$\frac{\partial b}{\partial t} + P\frac{\partial b}{\partial x} = \frac{\partial^2 b}{\partial x^2} - D\frac{b(1-b)}{\kappa + b}$$

$$\frac{\partial c}{\partial t} + P\frac{\partial c}{\partial x} = \frac{\partial^2 c}{\partial x^2} - \hat{D}\frac{b(1-b)}{\kappa + b} + S(1-c)$$

where the tildes and capitalization of the variables are omitted to obtain (1.4) and (1.5).

Acknowledgements. I would like to thank Dr. Hermann J. Eberl for his guidance and support as both a professor and project advisor.

REFERENCES

[1] D. G. Aronson and H. F. Weinberger, *Multidimensional nonlinear diffusion arising in population genetics*, Advances in Mathematics, 30 (1978), pp. 33–76.

[2] H. B. Braun and P. M. Berthouex, *Analysis of lag phase BOD curves using the monod equations*, Water Resources Research, 6 (1970), pp. 838–844, https://doi.org/10.1029/WR006i003p00838.

[3] H. Cai, A. Ghazaryan, and V. Manukian, *Fisher-kpp dynamics in diffusive rosenzweig–macarthur and holling–tanner models*, Mathematical Modelling of Natural Phenomena, 14 (2019), p. 404.

[4] R. Dresnack and W. E. Dobbins, *Numerical analysis of BOD and DO profiles*, Journal of the Sanitary Engineering Division, 94 (1968), pp. 789–807, https://doi.org/10.1061/JSEDAI.0000891.

[5] P. C. Fife, *Mathematical aspects of reacting and diffusing systems*, vol. 28, Springer Science & Business Media, 2013, https://doi.org/10.1007/978-3-642-93111-6.

[6] R. A. Fisher, *The wave of advance of advantageous genes*, Annals of eugenics, 7 (1937), pp. 355–369.
[7] A. R. Ghazaryan, S. Lafortune, and V. Manukian, *Introduction to Traveling Waves*, CRC Press, 2022, https://doi.org/10.1201/9781003147619.
[8] P. S. Hagan, *The instability of nonmonotonic wave solutions of parabolic equations*, Studies in Applied Mathematics, 64 (1981), pp. 57–88, https://doi.org/10.1002/sapm198164157.
[9] A. Kolmogorov, I. Petrovskii, and N. Piskunov, *A study of the diffusion equation with increase in the amount of substance, and its application to a biological problem.*, Selected Works of AN Kolmogorov, 1 (1937), https://doi.org/10.1201/9780367810504-7.
[10] C. C. Liu, P. Lin, and H. Xiao, *Water Environment Modeling*, CRC Press, 2021.
[11] J. D. Logan, *An introduction to nonlinear partial differential equations*, vol. 89, John Wiley & Sons, 2008.
[12] J. Monod, *Recherches sur la croissance des cultures bactériennes*, (1942).
[13] J. D. Murray, *Mathematical Biology*, Springer, 2002, ch. 13, pp. 437–483.
[14] D. H. Sattinger, *On the stability of waves of nonlinear parabolic systems*, Advances in Mathematics, 22 (1976), pp. 312–355.
[15] H. W. Streeter and E. B. Phelps, *A study of the pollution and natural purfication of the ohio river*, tech. report, US Department of Health, Education, & Welfare, 1925.
[16] The MathWorks Inc., *MATLAB*, 2024, https://www.mathworks.com/products/matlab.html (accessed 2024-06-06). Version: 24.1.0.2622093 (R2024a) Update 3.
[17] V. Volpert and S. Petrovskii, *Reaction–diffusion waves in biology*, Physics of life reviews, 6 (2009), pp. 267–310.
[18] J. Xin, *Front propagation in heterogeneous media*, SIAM review, 42 (2000), pp. 161–230.